frontiers in Materials

ORIGINAL RESEARCH
published: 09 September 2021
doi: 10.3389/fmats.2021.731449

Dynamic Triaxial Test and Microscopic Study of Solidified Muddy Soil With Different Mixing Ratios and Curing Ages

Zhou Chen[1], Haocheng Xu[1], Mayao Cheng[1]*, Hanwen Lu[1], Zhijian Wang[2] and Peiyu Feng[3]*

[1]School of Transportation and Civil Engineering & Architecture, Foshan University, Foshan, China, [2]China Railway Guangzhou Group Co., Ltd., Guangzhou, China, [3]China Railway Siyuan Survey and Design Group Co, Ltd., Wuhan, China

Aiming to explore the optimal mixture ratio and curing age of solidified muddy soil under dynamic load, the paper intends to investigate whether the solidified muddy soil can be used as filling of high-speed railway subgrade. Based on the dynamic triaxial test, the investigation measured the dynamic strain and dynamic elastic modulus of solidified muddy soil under different mix ratios and curing ages, and also observed the microscopic morphology of solidified muddy soil samples by using scanning electron microscope. The results show that the addition of cement and curing agent significantly increases the dynamic strength and elastic modulus of muddy soil, which effectively improve the dynamic characteristics of muddy soil. The curing effect of the curing agent is more obvious with the increase of the dosage of cement and curing agent under different mix ratio. The content of curing agent plays a leading role in the hydration reaction between cement, curing agent and soil particles. Additionally, in case of the same test conditions, when the ratio of cement mass to dry silt mass is 1:20, the ratio of diluent volume to dry silt mass is 1:20, with 28 days of curing age, its curing effect will reach the best.

Keywords: solidified muddy soil, dynamic triaxial test, mixture ratio, curing age, SEM

OPEN ACCESS

Edited by:
Yunchao Tang,
Guangxi University, China

Reviewed by:
Neven Ukrainczyk,
Darmstadt University of Technology, Germany
Jie Wu,
Wuhan Polytechnic University, China
Chang-Fu Hu,
East China Jiaotong University, China

****Correspondence:***
Zhou Chen
gscz19861985@fosu.edu.cn
Mayao Cheng
chengmayao@163.com

Specialty section:
This article was submitted to Structural Materials, a section of the journal Frontiers in Materials

Received: *27 June 2021*
Accepted: *31 July 2021*
Published: *09 September 2021*

Citation:
Chen Z, Xu H, Cheng M, Lu H, Wang Z and Feng P (2021) Dynamic Triaxial Test and Microscopic Study of Solidified Muddy Soil With Different Mixing Ratios and Curing Ages. Front. Mater. 8:731449. doi: 10.3389/fmats.2021.731449

INTRODUCTION

The construction goal of the Guangdong-Hong Kong-Macao Greater Bay Area is bound to promote the great development of railway construction in Guangdong's Pearl River Delta. However, the treatment and utilization of the rich deep muddy soil in Guangdong's Pearl River Delta has always been a difficulty in practical engineering application (Zhou, 2013). At present, the treatment methods of muddy soil include vacuum preloading (Yan et al., 2010), curing method (Radovanovic et al., 2016), electroosmosis (Tang et al., 2017), mixing pile (Yang et al., 2011), etc. Whereas, due to the limitations of its high-water content, high compressibility and low strength, many deficiencies and limitations in the practical engineering application existed in the present methods (Pan et al., 2020). The muddy soil shallow reinforcement technology that has emerged in recent years can better improve the shortcomings of the appeal method. The core construction method is to shallowly strengthen the extremely low-strength muddy soil through foundation treatment (Xu et al., 2019; Dong et al., 2011), and partly use fly ash (Sani et al., 2018; Karthik et al., 2014; Takhelmayum et al., 2013) and soil-fly ash-lime (Consoli et al., 2014) for reinforcement, thereby forming a hard shell layer and improving the bearing capacity of foundation. Judging from the existing research (Shan et al., 2021; Huang et al., 2010; Kuna et al., 2016), the shallow reinforcement technology of muddy soil can

be achieved by natural drying, sand-filled cushion, shallow soil drainage, and chemical reinforcement. The *in-situ* solidification method with solidifying agent can greatly reduce the cost and construction period, help to recycle industrial waste materials, and save the cost of spoiled land acquisition during the construction process and the cost of earthwork transportation, which is a new hot spot in the research of shallow reinforcement of muddy soil. Since the mechanical properties of the solidified muddy soil are affected by various factors such as natural environment and external excitation, the mechanical properties of the solidified muddy soil filler become complicated. Therefore, in order to further grasp the engineering characteristics of the solidified muddy soil and ensure that it can serve the construction and operation of the project, it is necessary to carry out research on the solidification performance of the solidified muddy soil.

The effect of railway trains on the muddy soil is mainly the cyclic dynamic load. Therefore, research on the dynamic performance of the solidified muddy soil under the train load, In order to clarify the change of solidification effect, to ensure the stability of mechanical properties of solidified muddy soil is the primary prerequisite to ensure the safe and stable operation of the train. Whereas, the solidified muddy under the train load, the microscopic properties of soil can greatly determine its macroscopic working properties. Therefore, combined with microscopic experiments to observe the structural properties of solidified muddy soils, it is a concentrated expression of its complex physical and mechanical properties. The available literature shows (Tian et al., 2020) that for solidified soils with different mix ratios and the same age conditions, the dynamic strength and dynamic elastic modulus are very different. In addition, age is also an important factor affecting the curing effect. Scholars at home and abroad have done abundant laboratory experiments on the theory of soil dynamic performance under load. For example, Sun et al. (2020) carried out dynamic triaxial tests on the muddy soil after multiple freeze-thaw cycles under negative temperature load, and found that the lower the temperature, the dynamic stress and dynamic modulus of the muddy soil under the freeze-thaw cycle. The conclusion that the influence of dynamic characteristics is more obvious; Wang et al. (2019) studied and analyzed the deformation and strength of solidified muddy soil under cyclic loading; Arulrajah et al. (2018) carried out experiments on unconfined compressive strength of solidified muddy soil with various moisture content, different amounts of cement curing agents, and different curing ages. Jian et al. (2013) took water glass as an auxiliary material for cement curing agents, and studied the effect of water glass on the improvement of the mechanical properties and impermeability of solidified soil (Amir-Faryar and Aggour, 2016); made research on the deformation process of silt-solidified soil under dynamic load conditions, and concluded that the time interval of load application is a factor affecting the deformation of solidified soil; Li et al. (2014) used indoor geotechnical tests and on-site construction conditions to systematically study the effects of cement, lime, and fly ash as soil solidification agents on soil solidification, and summarized the development law of the influence of the mixing amount and age of various materials on the performance indexes of soil engineering. Liang et al. (2020) took Guizhou red clay as the research object and observed the changes in the microstructure of the red clay with a scanning electron microscope (SEM); Zhang et al. (2021) used SEM to study the diametric splitting tests of compacted bentonite. In recent years, developed countries such as Europe, America and Japan have gradually applied the technology of solidified muddy soil in railway subgrade filling (Liu et al., 2018). However, due to the late start in China, the research on the mechanical properties of solidified soil mostly focuses on static forces. There are inadequate studies on characteristics. Particularly, the application of solidified soil in railway engineering is less extensive.

Therefore, the paper applies shallow silty soil in a coastal area of the Pearl River Delta as raw material soil, inorganic liquid curing agent and 32.5 ordinary Portland cement as additives, and uses SDT-10 microcomputer-controlled electro-hydraulic servo soil dynamic three-axis testing machine to solidify muddy soil. The study also carries out indoor dynamic triaxial tests of different mix ratios, and different ages by combing the SEM test to conduct microscopic observations of the loaded soil samples. Finally, the paper analyzes the dynamic strength and dynamics of the solidified muddy soil. The changing law of elastic modulus can obtain the best mixing ratio and curing age for curing effect, which provides theoretical basis for related engineering practice. We analyze the dynamic strength and dynamic elastic modulus of solidified muddy soil to obtain the best mix ratio and curing age of solidified muddy soil, which provides a theoretical basis for related engineering practice.

Test Plan

Due to the low confining pressure of the superficial subgrade filling, the loading frequency of the subgrade filling under the train load should be less than 1.85 Hz (Tian, 2020). Therefore, the confining pressure and axial pressure of the proposed sample are 100 kPa, the loading frequency is 1 Hz, the cycle number is 1,000 for the solidified muddy soil with changing mix ratio, and the cycle number is 400 for the solidified muddy soil with changing the curing age. Secondly, sine wave waveforms are used to simulate the repeated effects of railway trains on subgrade soil. In order to consider the real stress state of the shallow muddy soil, the test method is adopted in the test process to first carry out isobaric consolidation of the sample with a dynamic triaxial instrument. Afterwards, the study applies axial dynamic force. The specific test control data are shown in **Table 1**.

Test Materials and Test Preparation

The silt used in this experiment was taken from the shallow silt at the bottom of a pond in the Pearl River Delta region. The sampling depth is 0.5–3.0 m; the curing agent is "Xiyang Brand" F type liquid curing agent; the cement is 32.5 ordinary Portland cement. The operation steps of the sample preparation process refer to the specific methods in the *Regulations for Railway Engineering Geotechnical Tests* (TB 10102–2010). At the same time, since the undisturbed silt soil will inevitably be disturbed by the external environment during the sampling and

TABLE 1 | Test control conditions.

Dynamic strain	Confining pressure/kPa	Axial load amplitude/N	Vibration frequency/Hz	Drainage conditions	Vibration loading times/time	Wave
	100	**100**	**1**	**Undrained**	**1,000,00**	**Sine wave**
Dynamic elastic modulus	confining pressure/kPa 100	Axial load amplitude/N 100	Vibration frequency/Hz 1	Drainage conditions Undrained	Load level 10	Wave Sine wave

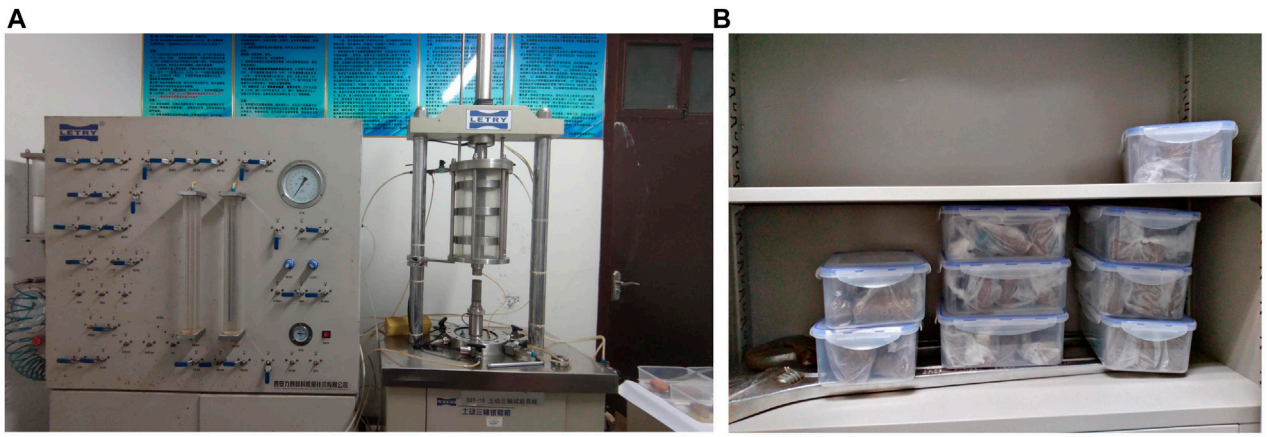

FIGURE 1 | Real scene of the equipment **(A)** SDT-10 microcomputer controlled electro-hydraulic servo soil dynamic triaxial testing machine **(B)** Scanning electron microscope.

transportation process. To eliminate the interference of the soil disturbance on the test results, the undisturbed muddy soil is reshaped before sample preparation. Further, the sample preparation is controlled. The moisture content is 30%, and the size of the prepared standard sample is diameter d = 39.1 mm, height h = 80 mm.

Sample Preparation Method

Firstly, the liquid curing agent and distilled water is diluted to a certain ratio to obtain the curing agent diluent. Further, the muddy soil to a constant weight is stored in a laboratory drying oven at 65°C, the dried muddy soil is pulverized into powder and by a pulverizer, that would pass through a 0.6 mm square hole sieve. Finally, powdery muddy soil is produced with a particle size of less than 0.6 mm. Additionally, the powdery silt is mixed with cement according to the proportion. The hardener diluent which is prepared in advance are added and more importantly mix them well. We prepare a number of solidified muddy soil standard samples with the sample preparation device, and put them in a plastic bag to wrap and seal the samples to cure to 7 days, 28 days and 90 days.

Test Equipment

Dynamic triaxial test equipment the SDT-10 microcomputer control electro-hydraulic servo soil dynamic triaxial testing machine which composed by seven parts, including axial pressure measurement and control system, confining pressure measurement and control system, pressure chamber, pressure chamber lifting mechanism, hydraulic oil source, electrical control system, computer display and control and data processing system, show in **Figure 1A**; Test Seal is saved as shown in **Figure 1B**.

TABLE 2 | Test mix ratio of solidified muddy soil.

Number	Cement mass g: dry sludge mass g	Diluent volume ml: dry sludge mass g
1	1:20	1:20
2	1:20	1:30
3	1:20	1:40
4	1:25	1:20
5	1:30	1:20

Tests on Dynamic Characteristics of Solidified Muddy Soil Under Different Mix Ratios

According to the above preparation being made, we equipped with standard test pieces of variable curing agent and cement content. In the experiment, a total of five sets of samples with different mix ratios were designed, with three parallel samples in each group. The specific mix ratios are shown in **Table 2**. The first group of curing age, they are 7, 28 days and 90 days respectively. Further, the maintenance age of the remaining groups was 28 days. According to < Standard for geotechnical testing

TABLE 3 | Cumulative strain change curve of different curing agent content under dynamic load.

Curing agent content	Cycles	1st test (mm)	2nd test (mm)	3rd test (mm)	Mean value (mm)	Standard deviation (%)
1:20	100	0.0175	0.0175	0.0184	0.0178	0.0424
	200	0.0182	0.0184	0.0181	0.0182	0.0125
	300	0.0186	0.0186	0.0183	0.0185	0.0141
	400	0.0183	0.0187	0.0188	0.0186	0.0216
	500	0.0184	0.0185	0.0195	0.0188	0.0497
	600	0.0189	0.0190	0.0188	0.0189	0.0082
	700	0.0196	0.0192	0.0185	0.0191	0.0455
	800	0.019	0.0188	0.0195	0.0191	0.0294
	900	0.0195	0.0195	0.0186	0.0192	0.0424
	1,000	0.0197	0.0194	0.0188	0.0193	0.0374
1:30	100	0.0232	0.0229	0.0224	0.0228	0.0330
	200	0.0244	0.0247	0.0256	0.0249	0.0510
	300	0.0263	0.0267	0.0265	0.0265	0.0163
	400	0.0276	0.0279	0.0267	0.0274	0.0510
	500	0.0283	0.0286	0.028	0.0283	0.0245
	600	0.0291	0.0296	0.028	0.0289	0.0668
	700	0.0292	0.0293	0.0297	0.0294	0.0216
	800	0.0301	0.0304	0.0293	0.0299	0.0464
	900	0.0302	0.0305	0.0299	0.0302	0.0245
	1,000	0.0303	0.0304	0.0311	0.0306	0.0356
1:40	100	0.0276	0.0276	0.0273	0.0275	0.0141
	200	0.0295	0.0295	0.0304	0.0298	0.0424
	300	0.0317	0.0315	0.0307	0.0313	0.0432
	400	0.0321	0.0325	0.0318	0.0321	0.0287
	500	0.0324	0.0325	0.0336	0.0328	0.0544
	600	0.0332	0.0328	0.034	0.0333	0.0499
	700	0.0339	0.0336	0.0339	0.0338	0.0141
	800	0.0342	0.0344	0.0338	0.0341	0.0249
	900	0.0348	0.035	0.0335	0.0344	0.0665
	1,000	0.0349	0.0347	0.0344	0.0347	0.0205

method > (GB/T 50,123–2019), We repeated each test for three times to show the scatters of the experimental results.

Test Results of Dynamic Characteristics of Solidified Muddy Soil Under Different Mix Ratios

Dynamic Strain Test Results

Table 3 and **Table 4** shows the cumulative strain of solidified Mucky soil under different mixing ratios and different cycles. From the data analysis in these tables, we can get the maximum value in the range of twice the average value plus the standard deviation, which shows that the test results are less discrete. **Figure 2** shows the cumulative strain curve of solidified muddy soil under different mixing ratios under different cycles. It can be seen from the figure that as the number of cycles increases, the cumulative strain of the sample also increases. In other words, the strain of the solidified silty soil is basically in a positive correlation with the number of cycles. Observing the development trend of the curve in the figure, it can be found out that the specimen compression is relatively large at the beginning of loading. When the number of cycles reaches a certain level, the strain growth rate of the specimen tends to slow down. This is because as the number of cycles increases, the inside of the sample gradually becomes dense. Whereas, the porosity inside the soil begins to decrease, the strength becomes higher and higher, and the corresponding strain begins to decrease.

From **Figure 2A**, it is easy to find that when the cement mass g is 1:20 than the dry sludge mass g, the cumulative strain is lower than 1:30 and 1:40. This is because as the content of the diluent increases, the crystals produced between the solidifying agent and the soil can make the connection between the soil particles closer. While the increase in molecular gravity makes many individual soil particles aggregate into small aggregates, thus forming a stable structure, the stiffness of the soil is improved. Therefore, the cumulative axial strain of the specimen becomes the smallest.

Comparing **Figure 2B**, when the cement mass g: dry sludge mass g is 1:20, the cumulative strain is lower than that at 1:30 and 1:40. The increase in cement content makes the contact between cement and curing agent closer, which results the hydrolysis and hydration reaction of cement and the liquid curing agent filling the pores in the soil structure well, thereby improving the stiffness of the silt soil.

Dynamic Elastic Modulus Test Results

The dynamic elastic modulus of silty soil refers to the relationship between the dynamic stress and the recoverable part of the

TABLE 4 | Cumulative strain change curve of different cement content under dynamic load.

Cement content	Cycles	1st test (mm)	2nd test (mm)	3rd test (mm)	Mean value (mm)	Standard deviation (%)
1:20	100	0.018	0.0181	0.0173	0.0178	0.0356
	200	0.018	0.0181	0.0185	0.0182	0.0216
	300	0.018	0.0181	0.0193	0.0185	0.0591
	400	0.019	0.019	0.0178	0.0186	0.0566
	500	0.0184	0.0187	0.0193	0.0188	0.0374
	600	0.0193	0.0188	0.0186	0.0189	0.0294
	700	0.0194	0.019	0.0189	0.0191	0.0216
	800	0.0194	0.019	0.019	0.0191	0.0189
	900	0.0189	0.0184	0.0202	0.0192	0.0759
	1,000	0.019	0.0189	0.02	0.0193	0.0497
1:25	100	0.0277	0.028	0.0281	0.0279	0.0170
	200	0.0325	0.0322	0.034	0.0329	0.0787
	300	0.036	0.0356	0.0373	0.0363	0.0726
	400	0.0395	0.0392	0.0386	0.0391	0.0374
	500	0.0413	0.0416	0.0413	0.0414	0.0141
	600	0.0433	0.043	0.0434	0.0432	0.0170
	700	0.0453	0.0456	0.0444	0.0451	0.0510
	800	0.0468	0.0464	0.0464	0.0465	0.0189
	900	0.0485	0.0482	0.0476	0.0481	0.0374
	1,000	0.0492	0.0493	0.0501	0.0495	0.0403
1:30	100	0.0255	0.0255	0.0257	0.0256	0.0094
	200	0.0268	0.0269	0.0274	0.0270	0.0262
	300	0.0281	0.0284	0.0272	0.0279	0.0510
	400	0.0282	0.0281	0.0295	0.0286	0.0638
	500	0.0289	0.0289	0.0298	0.0292	0.0424
	600	0.03	0.0301	0.029	0.0297	0.0497
	700	0.0299	0.0304	0.0301	0.0301	0.0205
	800	0.0306	0.0305	0.0307	0.0306	0.0082
	900	0.0313	0.0315	0.0301	0.0310	0.0618
	1,000	0.0309	0.0306	0.0325	0.0313	0.0834

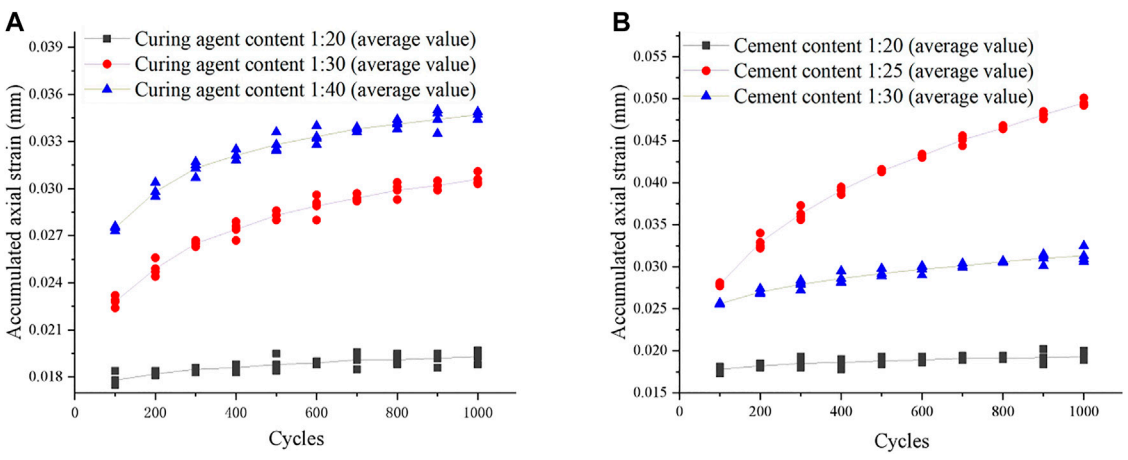

FIGURE 2 | Cumulative strain change curve of sample under dynamic load amplitude N = 100N and different cycle times **(A)** Different curing agent content **(B)** Different cement content.

dynamic strain in the soil (Oh and Vanapalli, 2014). Due to the periodic action of the dynamic load, a series of hysteretic curves appear between the dynamic stress and the dynamic strain. We also calculated the dynamic elastic modulus according to **formula (1)**:

$$E_d = \frac{\delta_{max} - \delta_{min}}{\varepsilon_{max} - \varepsilon_{min}} \quad (1)$$

In **formula (1)**, δ_{max}, δ_{min}, ε_{max}, and ε_{min} are the maximum and minimum values of stress and strain in the hysteresis curve,

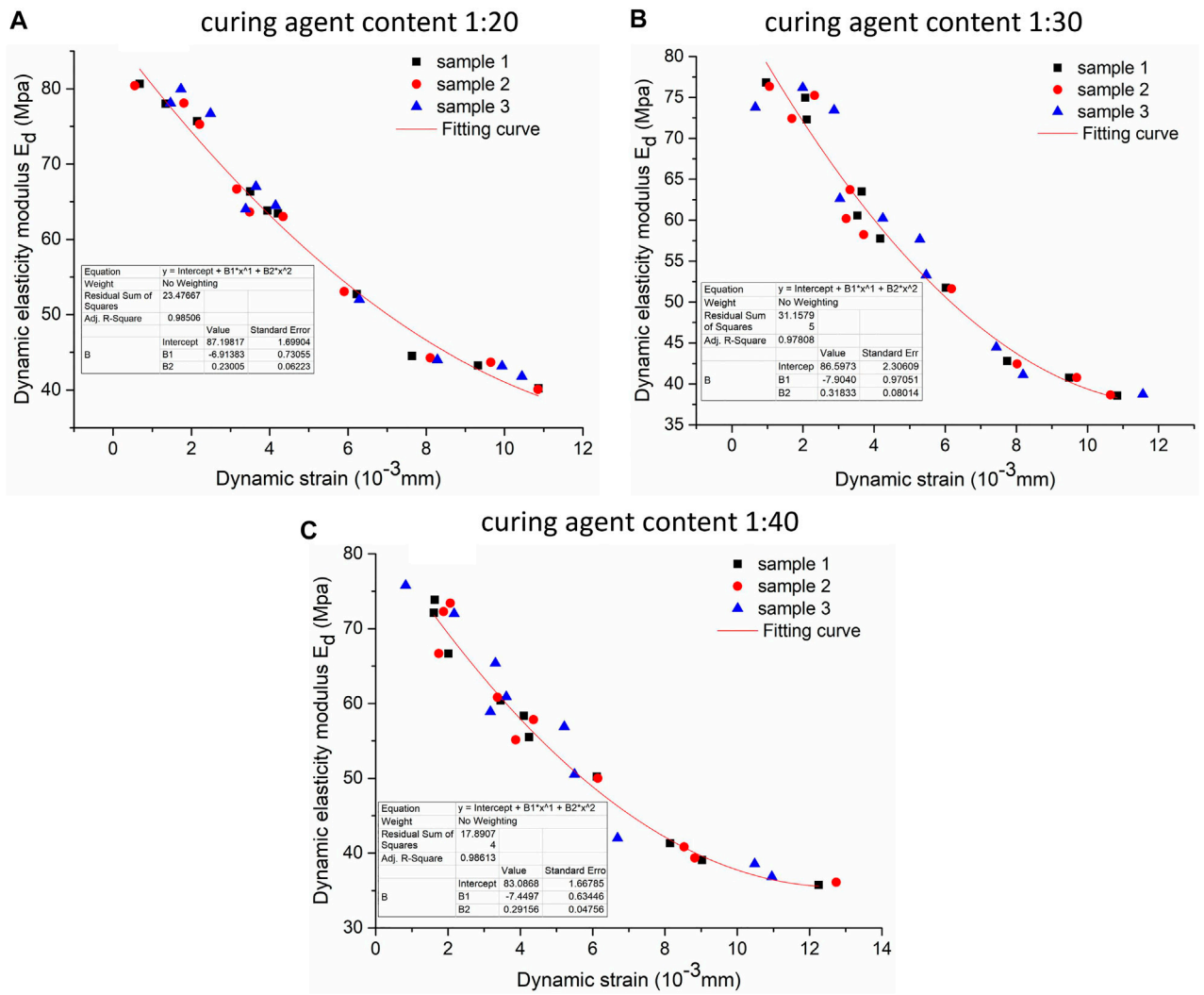

FIGURE 3 | Ed-εd relation curve under dynamic load amplitude N = 100N and different loading stages, Different curing agent content.

respectively. Firstly, we sort the E_d-ε_d data obtained in the experiment, as shown in **Figure 3** and **Figure 4**.

Figure 3 and **Figure 4** show the relationship between dynamic elastic modulus and dynamic strain of solidified muddy soil under different mix ratios. It can be included from the figure that the E_d-ε_d relationship curve of the solidified muddy soil under different mix ratios has the same trend, but the corresponding initial dynamic elastic modulus are different, and the specimens with high cement and curing agent content are initially elastic modulus is higher, indicating that as the amount of cement and curing agent increases, the initial dynamic elastic modulus of the solidified muddy soil can be effectively improved; As the number of loading stages increases, the corresponding dynamic strain increases and the dynamic elastic modulus decreases.

Comparing **Figure 3** and **Figure 4**, it can be found that when the ratio of cement mass to dry sludge mass is 1:20, and the ratio of diluent volume to dry sludge mass is 1:20, the sample produced lower strain under the same conditions. Because the higher the content of cement and curing agent, the higher the content of hydration products in the solidified muddy soil, the stronger the cementing force between soil particles, the denser the sample, the higher its stiffness, and the mechanical properties of the material are optimized, so the ability of the soil to resist deformation is enhanced. If the loading order increases, the sample becomes more and more hardened, Therefore its elastic deformation decreases, plastic deformation increases, and the dynamic elastic modulus decreases.

Test Results of Dynamic Characteristics of Solidified Muddy Soil Under Different Curing Ages

Table 5 shows the analysis of dynamic load amplitudes and final axial strain data of solidified muddy soil under different curing ages. From the table, the maximum values can be obtained in the

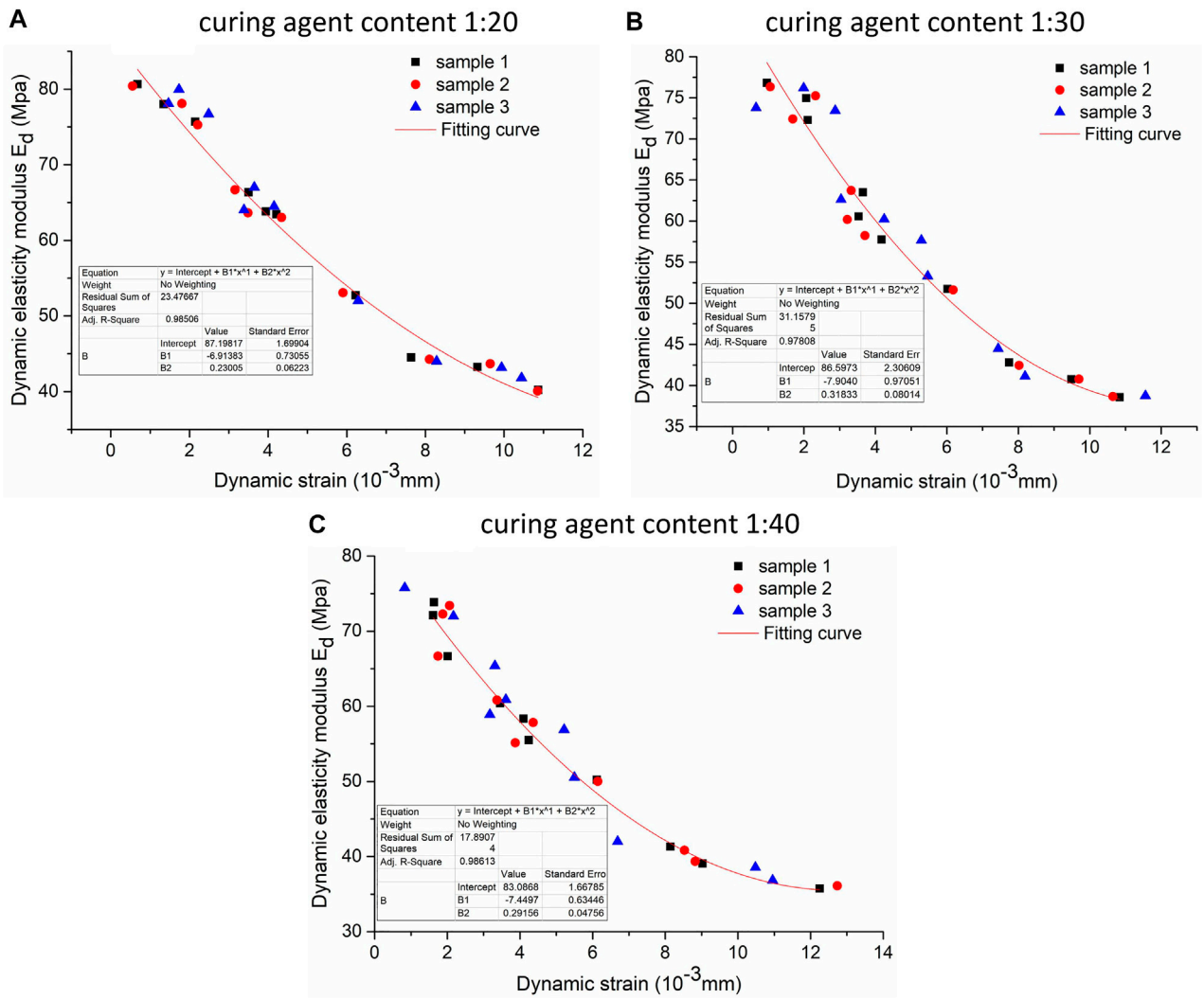

FIGURE 4 | Ed-εd relation curve under dynamic load amplitude N = 100N and different loading stages, Different cement content.

TABLE 5 | Final axial strain of solidified muddy soil at different curing ages.

Curing ages (d)	Amplitude (N)	1st test (mm)	2nd test (mm)	3rd test (mm)	Mean value (mm)	Standard deviation (%)
7	20	0.0048	0.0047	0.0059	0.0051	0.0544
	40	0.0076	0.0078	0.0087	0.0080	0.0478
	60	0.0211	0.0215	0.0204	0.0210	0.0455
	80	0.0288	0.0288	0.0276	0.0284	0.0566
	100	0.0332	0.0329	0.0339	0.0333	0.0419
28	20	0.0027	0.0022	0.0023	0.0024	0.0216
	40	0.0043	0.0041	0.0033	0.0039	0.0432
	60	0.006	0.0063	0.0061	0.0061	0.0125
	80	0.0093	0.0093	0.0082	0.0089	0.0519
	100	0.0118	0.0116	0.0129	0.0121	0.0572
90	20	0.0027	0.0028	0.0041	0.0032	0.0638
	40	0.0047	0.005	0.005	0.0049	0.0141
	60	0.0068	0.0071	0.0074	0.0071	0.0245
	80	0.0114	0.0118	0.0125	0.0119	0.0455
	100	0.0165	0.0168	0.0159	0.0164	0.0374

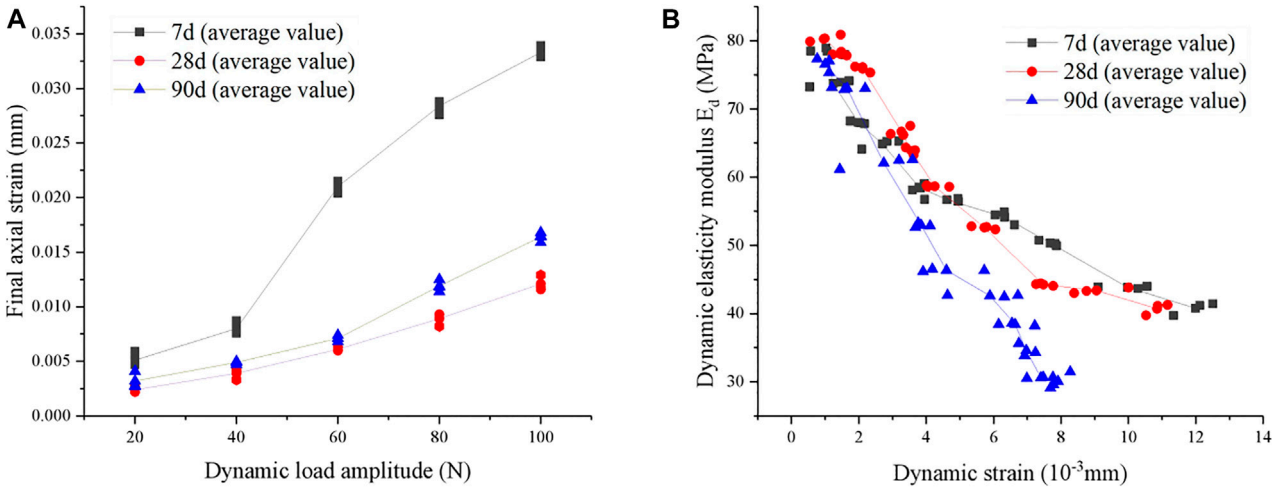

FIGURE 5 | Dynamic characteristics of solidified muddy soil at different curing ages **(A)** The curve between dynamic load amplitude and final axial strain **(B)** The curve between dynamic strain and dynamic elastic modulus.

range of two times the average value plus the standard deviation, it shows that the test results are less discrete. **Figure 5** shows the dynamic characteristics of solidified muddy soil under different curing age conditions. It can be seen from **Figure 5A** that with the increase of the dynamic load amplitude, the final axial strain of the solidified muddy soil also increases. More importantly, the final axial strain increases at different ages. When the final axial strain at 7 days is the largest, followed by 90 days, and the smallest at 28 days. Due to the hydration reaction between cement, curing agent, and muddy soil is slow, the reaction is insufficient when the curing age is 7 days. Consequently, the main effect of the early strength improvement is the physical filling effect. As the curing age reaches 28 days, the hydration reaction between cement, curing agent, and muddy soil is sufficient, which results those colloidal crystals fill and connect the molecular gaps between the soil well, improving the compactness of the muddy soil. Therefore, the strength of the solidified muddy soil continues to increase. Whereas, when the curing age reaches 90days, the rigidity of the solidified muddy soil begins to decrease, indicating that the curing effect of the curing agent is not indefinite. At last, the increase in age makes the curing agent possible to fail.

Table 6 shows the data analysis table of dynamic strain and dynamic modulus of elasticity of solidified muddy soil under different curing ages. From the table, the maximum relative error is 16.81% (curing ages 90 days), which shows that the experimental results are less discrete, the relative error and dispersion increase with the increase of age, indicating that the curing state becomes dispersed when the age reaches 90 days. According to **Figure 5B**, it can be inferred that when the curing age is 28 days, the initial dynamic elastic modulus of solidified muddy soil is larger than that of 7 days and 90 days. In cast that the curing age is 7 days, the hydration reaction between cement, curing agent, and muddy soil is insufficient. Further, the early stiffness improvement is mainly due to physical diffusion, the degree of improvement is therefore not obvious. When the curing age is 90 days, the dynamic elastic modulus of solidified silty soil tends to decrease over time. That is to say, the effect of the curing agent is weakened. Comparing the three curing ages, in case of dynamic elastic modulus of high solidified silty soil corresponding to 28 days, and the dynamic strain is the lowest, indicating that curing age of 28 days solidified muddy soil has the best hydration reaction effect. The gelling material greatly improves the cohesion between molecules, thereby effectively inhibiting the deformation of the silt soil particles.

Kang et al. (2017) showed that the dynamic constitutive relationship of soil under cyclic loading conforms to the following hyperbolic relationship through a large number of experimental studies, where:

$$\boldsymbol{\delta_d} = \frac{\boldsymbol{\varepsilon_d}}{\boldsymbol{a} + \boldsymbol{b\varepsilon_d}} \tag{2}$$

In **formula (2)**, where δ_d is the dynamic stress, ε_d is the elastic dynamic strain, and a and b are the soil parameters. On basis of **formula (2)**, $1/E_d = a+b\varepsilon_d$ can be obtained, that is, the reciprocal of dynamic elastic modulus has a linear relationship with the magnitude of dynamic strain. Therefore, we accordingly draw the correlation curve of $1/E_d \sim \varepsilon_d$, as shown in **Figure 6**.

It can be concluded from **Figure 6** that the test points fit with the straight line well. However, it should be noted that the dispersion is very small, indicating that the curves are basically linear for solidified muddy soils of different ages under the same test conditions. The larger the slope, the faster the dynamic strain increases, and the faster the reciprocal of the dynamic elastic modulus increases, that is, the faster the dynamic elastic modulus decreases. The hyperbolic model can well reflect the relationship between the strain of solidified silt and the dynamic elastic modulus. From **Figure 6**, the curve slope of 28 days solidified muddy soil is smaller than that of 7 days and 90 days solidified muddy soil, its dynamic elastic modulus is therefore larger than that of the other two groups of solidified muddy soil, indicating that 28 days is the curing age with the best curing agent effect.

TABLE 6 | Dynamic elasticity modulus E_d of solidified muddy soil at different curing ages.

Curing ages (d)		Dynamic strain (10^{-3}mm)	Actual measurement E_d (Mpa)	Regression analysis E_d (Mpa)	Relative error (%)
7	1st test	1.025	78.904	74.427	6.02
		1.462	73.901	72.147	2.43
		2.165	67.841	68.650	1.18
		3.182	65.269	63.961	2.04
		3.589	58.128	62.208	6.56
		4.942	56.837	56.881	0.08
		6.046	54.444	53.109	2.51
		7.345	50.754	49.331	2.89
		10.279	43.671	43.425	0.57
		12.12	41.183	41.580	0.95
	2nd test	0.569	78.48	76.891	2.07
		1.71	74.119	70.890	4.56
		1.74	68.224	70.740	3.56
		2.832	65.247	65.526	0.43
		3.829	58.39	61.206	4.60
		4.947	56.446	56.863	0.73
		6.312	54.891	52.277	5.00
		7.819	50.277	48.130	4.46
		10.548	43.973	43.066	2.11
		12.505	41.419	41.375	0.11
	3rd test	1.579	77.951	71.551	8.94
		0.539	73.229	77.057	4.97
		2.057	67.929	69.174	1.80
		2.086	64.094	69.033	7.15
		3.943	59.033	60.739	2.81
		3.95	56.739	60.711	6.54
		6.617	53.015	51.360	3.22
		7.861	49.953	48.028	4.01
		9.098	43.891	45.364	3.25
		11.339	39.722	42.187	5.84
28	1st test	0.55	79.869	85.285	6.35
		1.223	77.985	79.858	2.34
		2.109	76.122	73.248	3.92
		3.32	66.193	65.196	1.53
		3.666	63.933	63.104	1.31
		4.016	58.763	61.082	3.80
		5.786	52.699	52.308	0.75
		7.4	44.417	46.422	4.32
		8.756	43.32	43.035	0.66
		10.867	41.129	40.595	1.31
	2nd test	0.955	80.261	81.977	2.09
		1.636	77.822	76.701	1.46
		1.89	76.186	74.825	1.82
		2.942	66.316	67.587	1.88
		3.395	64.316	64.734	0.65
		4.053	58.592	60.873	3.75
		6.047	52.339	51.220	2.18
		7.259	44.305	46.856	5.44
		8.388	42.999	43.814	1.86
		11.162	41.258	40.529	1.80
	3rd test	1.459	80.881	78.038	3.64
		1.477	78.379	77.901	0.61
		2.337	75.328	71.645	5.14
		3.523	67.513	63.957	5.56
		3.624	63.229	63.353	0.20
		4.681	58.589	57.501	1.89
		5.342	52.786	54.281	2.75
		7.766	44.05	45.368	2.90
		10.006	43.806	41.174	6.39
		10.521	39.743	40.759	2.49
90	1st test	1.116	77.044	74.376	3.59
		1.571	72.883	70.620	3.20
		3.189	62.487	58.239	7.29

(Continued on following page)

TABLE 6 | (*Continued*) Dynamic elasticity modulus E_d of solidified muddy soil at different curing ages.

Curing ages (d)		Dynamic strain (10^{-3}mm)	Actual measurement E_d (Mpa)	Regression analysis E_d (Mpa)	Relative error (%)
		4.113	52.869	51.853	1.96
		4.178	46.531	51.422	9.51
		6.316	42.45	38.633	9.88
		6.148	38.417	39.541	2.84
		7.238	34.308	33.939	1.09
		6.984	30.515	35.182	13.27
		7.773	29.594	31.442	5.88
	2nd test	0.761	77.344	77.391	0.06
		1.196	73.138	73.707	0.77
		3.593	62.572	55.386	12.97
		3.762	53.291	54.220	1.71
		3.903	46.175	53.261	13.30
		6.719	42.659	36.520	16.81
		6.544	38.587	37.426	3.10
		6.917	33.865	35.517	4.65
		7.47	30.676	32.835	6.58
		7.685	29.113	31.841	8.57
	3rd test	1.114	75.319	74.393	1.24
		2.183	73.014	65.758	11.03
		1.432	61.151	71.755	14.78
		3.675	52.615	54.818	4.02
		5.72	46.305	41.930	10.43
		4.628	42.691	48.509	11.99
		7.219	38.22	34.030	12.31
		6.746	35.628	36.382	2.07
		7.758	30.663	31.510	2.69
		8.272	31.445	29.263	7.46

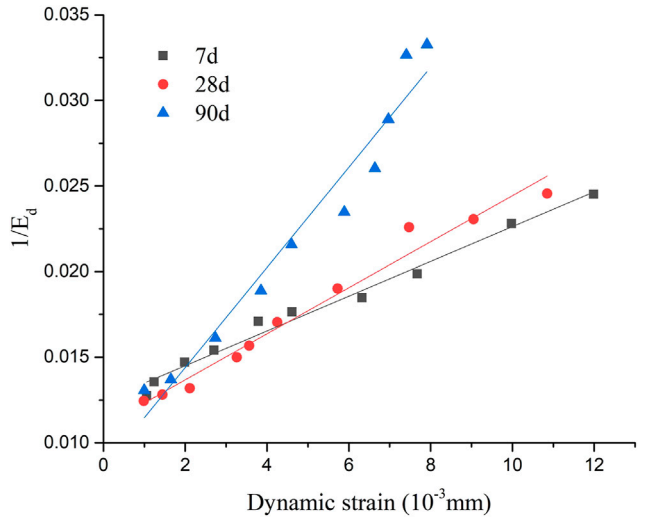

FIGURE 6 | Relationship curve of $1/E_d$~ε_d of solidified muddy soil at different curing ages.

INDOOR SCANNING ELECTRON MICROSCOPE MICROSCOPIC TEST

Test Principle and Scheme

In the experiment, through sampling the samples after the moving strain test and scanning electron microscopy test, the paper studies the quantitative structural characteristics of the solidified muddy soil by selecting typical sample maps aiming to reveal the microstructure characteristics of the solidified muddy soil. With the purposed of avoiding disturbing the structure of solidified muddy soil, we collected the powder samples with a surface thickness of about 3 mm with a soil cutter and placed in a sealed sample box. Furthermore, to eliminate the interference of moisture and the vacuum degree of the SEM vacuum system on the test results, it is necessary to dry the samples, so the samples were dried in an 80°C oven, and then transported back to the laboratory for SEM test observation. More specific experimental steps are as follows:

1) Take a powder sample with a thickness of about 3 mm on the surface of the test block after the dynamic triaxial test.
2) Put the powdered sample in the plastic box, label it and put it in the drying box for drying.
3) Sprinkle the powdered sample evenly on the sample stage, and use a scanning electron microscope (SEM) to scan and image the surface of the sample point by point.

Legend of the Sample Observed in the Test

Figures 7, **8** present examples of samples under different mixing ratios. It is shown from **Figure 7** with the increase of content of curing agent, curing muddy soil skeleton structure of microscopic particles form starts from single chip sorting clutter to sort stereospecificity obvious granular, which shows that with the increase of content of curing agent, cement, curing agent. The

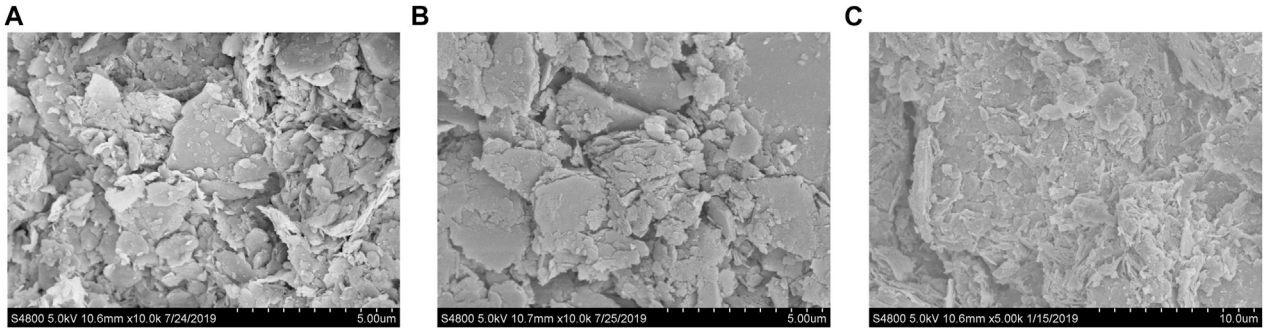

FIGURE 7 | SEM images of solidified muddy soil with different curing agent contents **(A)** Curing agent content (1:40) **(B)** Curing agent content (1:30) **(C)** Curing agent content (1:20).

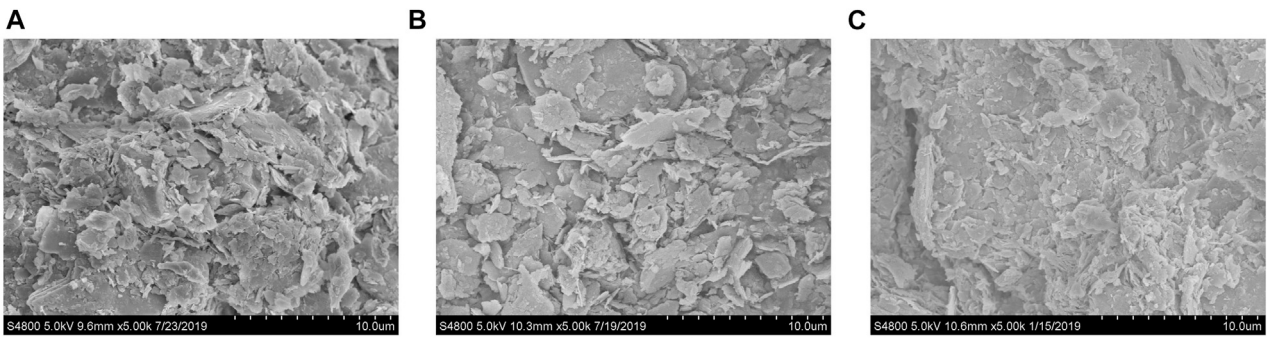

FIGURE 8 | SEM images of solidified muddy soil with different cement contents **(A)** Cement content (1:30) **(B)** Cement content (1:25) **(C)** Cement content (1:20).

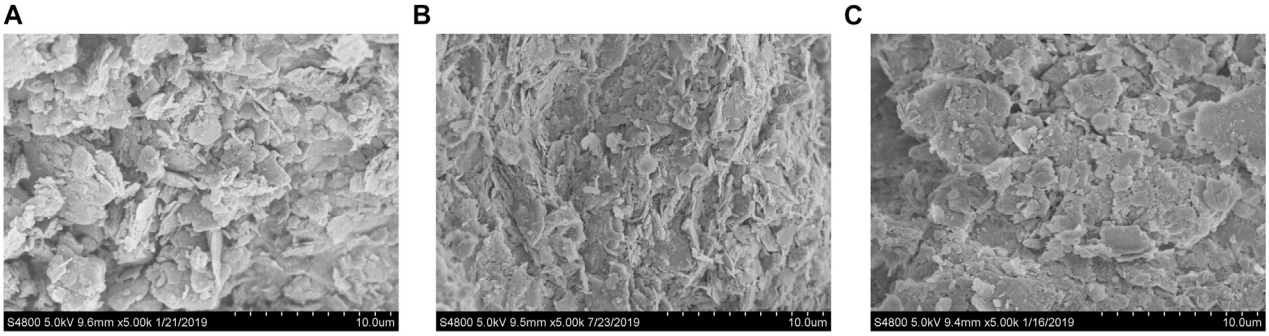

FIGURE 9 | SEM images of solidified muddy soil at different curing ages **(A)** 7 days **(B)** 28 days **(C)** 90 days

hydration reaction between soil particles can effectively adhere to the soil particle. It acts as a connecting "bridge" to fill in the particle gap, thus improving the structural properties of the solidified silty soil itself.

It is clear from **Figure 8**, following the increase of cement content, the contact area of the solidified mud soil microscopic particles started from dot and gradually become section. It is noted that the contact area increases. This is because the cement content increase cement, curing agent, hydration gel between the soil particles will flake silt particle conglomerate, particle clearance gradually be populated, internal close-grained, to form a whole structure. On the macroscopic level, the strength and stiffness of solidified silty soil are enhanced.

By comparing **Figure 7** and **Figure 8**, it can be concluded that the influence of content of curing agent on solidified silty soil is greater than that of changing the content of cement. This is because the content of curing agent plays a leading role in the

hydration reaction between cement, curing agent and soil particles. On another hand, the increasing curing agent content can effectively promote the growth of hydration gel products.

Figure 9 is an example of samples under different curing age conditions. It is found out that the curing age is 7 days. Consequently, the microstructure of solidified muddy soil presents a large number of flaky particles piled up. The surface of the soil particles is very rough, coupling with a lot of gaps in the internal structure. However, as the curing age reaches 28 days, a large amount of hydration gel material condenses the flaky particles. Especially, the hydration products penetrate into the interstices of the internal structure of the soil, bonding the soil particles together and making the surface relatively flat and smooth. While the curing age reaches 90 days, it will result in mutual slippage between the polymers. In this case, a small amount of rough monolithic particles appears, indicating that the curing effect decreases with the curing age reaching 90 days.

Dynamic triaxial test and SEM microscopic tests were combined to analyze the relationship of the solidified muddy and the mechanic property. From section 4 and section 5, we will find that there exists proportional relationship between micro-structure and mechanical property. On the one hand, the solidified muddy will change the structure by filling the particle gap, thus raising the compactness degree of soil. On the other hand, the cementation of the solidified muddy can effectively adhere the soil particles, thus raising the cohesive force of soil. The compactness degree and the cohesive force affect proportionally the dynamic elastic modulus and dynamic strain of the soil.

CONCLUSION

Through indoor dynamic triaxial test and SEM microscopic test on solidified muddy soil, the paper analyzes the influence of changing mix ratio and curing age on solidification effect according to the test results of dynamic characteristics of solidified muddy soil with different mix ratio and curing age. The corresponding conclusions are drawn as following:

1) Under the conditions of different mix ratios, with the increase in the mixing amount of cement and curing agent, the curing effect of the curing agent is more obvious. Particularly, the curing agent content dominates in the hydration reaction between cement, curing agent and soil particles. The mixing of cement and curing agent significantly improves the dynamic strength and dynamic elastic modulus of the powdery silty soil, and can effectively improve the dynamic characteristics of the powdery silty soil.
2) With the increase of the loading series, the corresponding dynamic strain increases. Whereas, the dynamic elastic modulus shows a downward trend. Particularly, the dynamic cohesion inside the structure increases, the soil gradually becomes compact, and its stiffness increases.
3) The theoretical curve predicted by adopting the hyperbolic model can fit with the relationship between dynamic stress and dynamic strain of solidified silty soil well.
4) The results show that the best mix ratio can be obtained when the ratio of cement mass to dry sludge mass is 1:20, additionally the ratio of diluent volume to dry sludge mass is 1:20. There is no adhesion between the particles in the silt soil sample, with only friction between the particles and the inlaid bite. After mixing cement and curing agent, part of the hydration products are wrapped on the surface of the soil particles in flocculent or fibrous form. Moreover, some hydration products fill the pores between the soil particles. However, with the increase of age, the hydration products stretch to the soil particles. Interstitials or pores between sand particles extend and overlap and begin to agglomerate. When its age reaches 28 days, the agglomeration is enhanced. Therefore, a grid-like spatial skeleton structure is gradually formed, which binds the soil particles into one body and strengthens the soil particles. The connection between the two has realized the improvement of the mechanical properties of the silt soil.
5) The solidifying agent strengthens the silt as the base layer or subbase layer of the road pavement. Additionally, its strength increases faster and more stable in the early stage, with a higher resistance to deformation. In coastal areas where silt soil is widely distributed, it is practical to use curing agent to reinforce the silt soil as the base or subbase of high-speed railway station buildings and railways. The research can solve the resource shortage problems such as insufficient fillers and stones. More importantly, the *in-situ* solidification can effectively reduce the damage to the natural environment, and achieve energy saving and reduction by recycling resources.
6) The paper basically focuses on the investigation of agitated silt soil to obtain regular conclusions. But the silt sample undergoes drying, crushing and other pretreatment operations, which may change some properties and cause a certain difference in the effect of silt *in-situ* solidification. It's necessary to be further studied regarding on the effect mechanism of curing agent on different silt soils and whether the effect is the same. The research on the mechanical properties of silt is limited to dynamic characteristics. While, it needs to be further studied on the changing laws of certain static mechanical indexes such as unconfined compressive strength, partial shear strength, compressibility, stability, etc. The future research is generally divided into two steps: 1) To further deepen the research on curing effect durability, 2) To further carry out research on on-site quality control approach combined with engineering practice so as to provide a more comprehensive theoretical basis for high-quality construction of actual projects.

DATA AVAILABILITY STATEMENT

The raw data supporting the conclusions of this article will be made available by the authors, without undue reservation.

AUTHOR CONTRIBUTIONS

ZC: Data curation, Formal analysis, Investigation,Methodology, Software,Visualization, Writing.—review and editing. HX: Formal analysis, Validation,Writing-review and editing. MC Formal analysis, Investigation,Methodology,Writing-original draft. HL: Data curation, Funding acquisition. ZW: Project administration. PF: Validation.

FUNDING

The work described in this paper was financially supported by the National Natural Science Foundation of China (Grant No. 51908146), Characteristic innovation projects of colleges and universities in Guangdong Province (2019KTSCX190) the Foshan self-funded science and technology plan project (Grant No. 1920001001539).

REFERENCES

Amir-Faryar, B., and Aggour, M. S. (2016). Effect of Fibre Inclusion on Dynamic Properties of clay. *Geomechanics and geoengineering* 11 (2), 104–113. doi:10.1080/17486025.2015.1029013

Arulrajah, A., Yaghoubi, M., Disfani, M. M., Horpibulsuk, S., Bo, M. W., and Leong, M. (2018). Evaluation of Fly Ash- and Slag-Based Geopolymers for the Improvement of a Soft marine clay by Deep Soil Mixing. *Soils and foundations* 58 (6), 1358–1370. doi:10.1016/j.sandf.2018.07.005

Consoli, N. C., da Rocha, C. G., and Silvani, C. (2014). Devising Dosages for Soil-Fly Ash-Lime Blends Based on Tensile Strength Controlling Equations. *Construction Building Mater.* 55 (Mar.), 238–245. doi:10.1016/j.conbuildmat.2014.01.044

Dong, Z. L., Zhang, G. X., Zhou, Q., Luo, Y., Qiu, Q., Li, Y., et al. (2011). RESEARCH AND APPLICATION OF IMPROVEMENT TECHNOLOGY OF SHALLOW ULTRA-SOFT SOIL FORMED BY HYDRAULIC RECLAMATION IN TIANJIN BINHAI NEW AREA. *Chin. J. Rock Mech. Eng.* 30 (005), 1073–1080. CNKI:SUN:YSLX.0.2011-05-027.

Huang, Y., Zhou, Z. Z., and Bo, J. (2010). Micro-experiments on a Soft Ground Improved by Cement-Mixed Soils with gypsum Additive. *Chin. J. Geotechnical Eng.* 32 (08), 1179–1183.

Jian, W. B., Sun, D., and Huang, C. X. (2013). Micromechanism of Cement-Sodium Silicate-Stabilized Soft Soils. *Chin. J. Geotechnical Eng.* 35 (S2), 632–637.

Kang, G.-o., Tsuchida, T., and Kim, Y.-s. (2017). Strength and Stiffness of Cement-Treated marine Dredged clay at Various Curing Stages. *Construction Building Mater.* 132 (FEB.1), 71–84. doi:10.1016/j.conbuildmat.2016.11.124

Karthik, S., Ashok, K., Gowtham, P., Elango, G., Gokul, D., and Thangaraj, S. (2014). Soil Stabilization by Using Fly Ash. *IOSR J. Mech. Civil Eng.* 10 (6), 20–26. doi:10.9790/1684-1062026

Kuna, K., Airey, G., and Thom, N. (2016). Development of a Tool to Assess *In-Situ* Curing of Foamed Bitumen Mixtures. *Construction Building Mater.* 124, 55–68. doi:10.1016/j.conbuildmat.2016.07.086

Li, H. L., Liu, K., and Shen, Y. (2014). Experimental Research on Road-Used Performance of Dredger Fill with Cement-Lime Curing. *J. Water Resour. Architectural Eng.* 12 (02), 51–57. doi:10.3969/j.issn.1672-1144.2014.02.011

Liang, S. H., Lu, Y. D., Pan, W. S., and Xiaozhou, Z. (2020). Study on Microstructure of Red Clay in Southern Guizhou Province Based on SEM. *Water Resour. Power* 38 (02), 151–154. CNKI:SUN:SDNY.0.2020-02-038.

Liu, S. Y., Zhang, T., and Cai, G. J. (2018). Research on Technology and Engineering Application of Silt Subgrade Solidified by Lignin-Based Industrial By-Product. *China J. Highw. &Transport* 31 (3), 1–11. doi:10.19721/j.cnki.1001-7372.2018.03.001

Oh, W. T., and Vanapalli, S. K. (2014). Semi-empirical Model for Estimating the Small-Strain Shear Modulus of Unsaturated Non-plastic Sandy Soils. *Geotech Geol. Eng.* 32 (2), 259–271. doi:10.1007/s10706-013-9708-5

Pan, C., Xie, X., Gen, J., and Wang, W. (2020). Effect of Stabilization/solidification on Mechanical and Phase Characteristics of Organic River silt by a Stabilizer. *Construction Building Mater.* 236 (2), 117538. doi:10.1016/j.conbuildmat.2019.117538

Radovanovic, D. D., Kamberovic, Z. J., Korac, M. S., and Rogan, J. R. (2016). Solidified Structure and Leaching Properties of Metallurgical Wastewater Treatment Sludge after Solidification/stabilization Process. *Environ. Lett.* 51 (1-2), 34–43. doi:10.1080/10934529.2015.1079104

Sani, A., Muhammad, N. Z., Mehan, A., and Joel, M. (2018). Optimization of Fly-Ash Dosage for the Stabilization of Gravel Soil Using Cement for Use as Flexible Pavement Material. *Adv. Sci. Lett.* 24 (6), 3914–3917. doi:10.1166/asl.2018.11510

Shan, W., Chen, H.-e., Yuan, X., Ma, W., and Li, H. (2021). Mechanism of Pore Water Seepage in Soil Reinforced by Step Vacuum Preloading. *Bull. Eng. Geol. Environ.* 80 (3), 2777–2787. doi:10.1007/s10064-020-02075-4

Sun, J., Gong, M. S., and Xiong, H. Q. (2020). Experimental Study of the Effect of Freeze-Thaw Cycles on Dynamic Characteristics of Silty Sand. *Rock Soil Mech.* 41 (03), 747–754. doi:10.16285/j.rsm.2019.0679

Takhelmayum, G., Savitha, A. L., and Gudi, K. (2013). Laboratory Study on Soil Stabilization Using Fly Ash Mixtures. *Int. J. Eng. Sci. Innovative Technol.* 2 (1), 477–482.

Tang, X., Xue, Z., Yang, Q., Li, T., and VanSeveren, M. (2017). Water Content and Shear Strength Evaluation of marine Soil after Electro-Osmosis Experiments. *Drying Technol.* 35 (14), 1696–1710. doi:10.1080/07373937.2016.1270299

Tian, Z. K. (2020). *Experimental Study and Numerical Simulation of Mechanical Properties of Solidified Silt Soil under Dynamic*. Ph. D. Thesis (Hengyang: University of south China).

Tian, Z. K., Peng, C., and Tan, Y. Q. (2020). Effect of Dynamic Action on Mechanical Properties of Composite Solidified Silt Soil. *J. Univ. South China(Science Technology)* 34 (02), 62–68. doi:10.19431/j.cnki.1673-0062.2020.02.010

Wang, J., Li, S., and Feng, T. (2019). A Method Analyzing Deformation of Anchor Foundations in Soft clay under Static and Cyclic Loads. *Appl. Ocean Res.* 84, 133–144. doi:10.1016/j.apor.2019.01.010

Xu, R. Q., Wang, X., Wen, J. Y., and Bingjian, Z. (2019). Curing Agent for Shallow Mucky Soil. *J. Shanghai Jiaotong Univ.* 53 (07), 805–811. doi:10.16183/j.cnki.jsjtu.2019.07.006

Yan, J., Wang, Q., and Zhang, J. (2010). Environmental Influence of Vacuum Preloading Dredging Project. *Proced. Environ. Sci.* 2, 1613–1621. doi:10.1016/j.proenv.2010.10.172

Yang, X. R., Zhang, L. Y., Li, H. C., and Dong, L. Y. (2011). Study and Analysis on Pile-Soil Stress Ratio of the Composite Foundation of Cement-Soil Mixing Pile under Flexible Foundation. *Amr* 335-336, 1145–1150. doi:10.4028/www.scientific.net/amr.335-336.1145

Zhang, J. R., Wang, L. J., Jiang, T., Zhao, J., Ren, M., Li, H., et al. (2021). Diametric Splitting Tests on Compacted Bentonite at Different High Suctions Based on PIV Technique. *J. Basic Sci. Eng.* 29 (03), 691–701. doi:10.16058/j.issn.1005-0930.2021.03.014

Zhou, H. (2013). *Study on Soft Soil Microstructure and Mechanism of Seepage and Consolidation in Pearl River Delta*. Ph. D. Thesis (Guangzhou: South China University of Technology).

Conflict of Interest: Author ZW, is employed by China Railway Guangzhou Group Co., Ltd. Author PF is employed by China Railway Siyuan Survey and Design Group Co, Ltd.

The remaining authors declare that the research was conducted in the absence of any commercial or financial relationships that could be construed as a potential conflict of interest.

Publisher's Note: All claims expressed in this article are solely those of the authors and do not necessarily represent those of their affiliated organizations, or those of the publisher, the editors and the reviewers. Any product that may be evaluated in this article, or claim that may be made by its manufacturer, is not guaranteed or endorsed by the publisher.